Magnetic domain structure and magneto-transport properties of laser ablated $Co_{40}Fe_{40}B_{20}$ thin films

Swamy, G. Venkat; Rout, P. K.; Pandey, Himanshu; Riscob, B.; Basheed, G. A.

DOI
10.1088/2632-959X/acfd46

Publication date
2023

Document Version
Final published version

Published in
Nano Express

PAPER • OPEN ACCESS

Magnetic domain structure and magneto-transport properties of laser ablated $Co_{40}Fe_{40}B_{20}$ thin films

To cite this article: G Venkat Swamy *et al* 2023 *Nano Ex.* **4** 045002

IOP Publishing Nano Express 4 (2023) 045002 https://doi.org/10.1088/2632-959X/acfd46

NANO EXPRESS

RECEIVED
27 June 2023

REVISED
21 September 2023

ACCEPTED FOR PUBLICATION
26 September 2023

PUBLISHED
13 October 2023

PAPER

Magnetic domain structure and magneto-transport properties of laser ablated $Co_{40}Fe_{40}B_{20}$ thin films

G Venkat Swamy[1,*], P K Rout[2], Himanshu Pandey[3], B Riscob[4] and G A Basheed[5]

[1] Department of Physics, St. John's College, M. G. Road, Agra, Uttar Pradesh 282002, India
[2] QuTech and Kavli Institute of Nanoscience, Delft University of Technology, 2600 GA Delft, The Netherlands
[3] Department of Physics, Sardar Vallabhbhai National Institute of Technology Surat, Ichchhanath, Keval Chowk, Surat- Dumas Road, Surat, Gujarat 395007, India
[4] Institute for Plasma Research, Bhat, Gandhinagar 382428, India
[5] EPR and Magnetic Fluids Group, Faculty of Physical Science, CSIR-National Physical Laboratory, 110012, New Delhi, India
[*] Author to whom any correspondence should be addressed.

E-mail: venkat@stjohnscollegeagra.in and venkatgrace1@gmail.com

Keywords: soft magneto crystalline materials, magnetic domain structure, magneto transport, ferromagnetic thin films

Abstract

We report the magnetic domain structure, and electrical and magnetoresistance properties of laser ablated $Co_{40}Fe_{40}B_{20}$ (CoFeB) (6 to 36 nm) thin films deposited on SiO_2 / Si(001) substrates. Magnetic force microscopy performed on annealed CoFeB thin films revealed larger magnetic domains, which are formed due to strong exchange coupling between the grains. The temperature-dependent sheet resistance of as-deposited thin films revealed that the observed non-metallic behavior is due to intragrain-tunneling and SiO_2 inclusions in the amorphous matrix. The metallic behavior of annealed CoFeB thin films is due to electron scattering from grain boundaries and granularity correlated to the formation of nano-crystallites. Thickness and field-dependent magneto-transport studies show higher magnetoresistance values for thinner annealed CoFeB films due to more scattering events upon crystallization, which is consistent with the granular nature of the annealed thin films.

1. Introduction

$Co_{40}Fe_{40}B_{20}$ (CoFeB) alloy thin films have been under extensive research focus due to their high tunneling magnetoresistance (TMR) which is utilized for spintronics applications such as magnetoresistive random-access memory [1, 2]. To improve the giant TMR, post-growth thermal annealing of the CoFeB layer and its chemical composition, crystalline structure as well as the magnetic structure are important topics of investigation in any device [3–12]. Moreover, it was reported that TMR can be enhanced by the amorphization of normally bcc CoFe alloy thin films sandwiched between two conventional amorphous materials [13]. Therefore, the basic understanding of the structural, electrical and magneto-transport properties of CoFeB thin films is essential for further improvement of spintronic devices.

Magnetoresistance (MR) of granular ferromagnet with non-magnetic metals and insulators such as Co-Ag and Co-SiO_2 etc, observed that electrical conduction properties are different although magnetic properties are similar [14–16]. An earlier study on transport anisotropy in CoFeB-SiO_2 granular amorphous thin films revealed that isotropic giant magnetoresistance (GMR) appears due to electrons hopping between granules [16, 17]. They found that electrical resistivity is lowered by applying a magnetic field and also has less anisotropic resistivity in the film with high metallic content. Moreover, the study on GMR of CoFeB-SiO_2 amorphous granular composites revealed the absence of MR for the samples with metallic content above 50% [17]. CoFeB/MgO granular system offers significantly high MR due to the magnetic softness of CoFeB thin films which undergo a ferromagnetic to superparamagnetic phase transition at 130 K [18]. However, an individual CoFeB with Ni nanotubes reported that the anisotropic MR values up to 1.4% at room temperature [19].

To investigate these aspects further, we have analyzed the magnetic domain structure and electrical and magneto-transport properties of CoFeB thin films of different thicknesses.

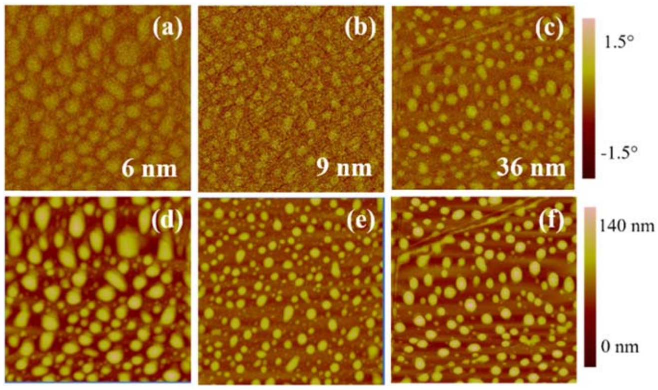

Figure 1. (a)—(c) The MFM images and the corresponding AFM images (d)—(f) with an area of 3 ×3 μm^2 for as-deposited CoFeB thin films of varying thicknesses 6, 9, and 36 nm respectively.

2. Experimental

We have employed pulsed laser deposition (PLD) technique as it offers a unique advantage for the growth of multi-elemental films of desired stoichiometry for the deposition of CoFeB thin films [20, 21] on SiO_2 (300 nm) / Si(001) substrates. The substrates are commercially available oxidized Si(001) wafers with a 300 nm thick SiO_2 seed layer. The oxide layer ensures the electrical isolation of the film from Si. A KrF excimer laser was used to ablate a stoichiometric target of $Co_{40}Fe_{40}B_{20}$ (at %). To enhance the crystallinity, the films were subsequently annealed at 400°C for 1 h in a high vacuum (1×10^{-6} Torr), immediately after deposition. For the post-growth annealing, the temperature increased to 200°C at 20°C per min and then from 200°C to 400°C at 10°C per min. Then we anneal the films at 400°C for 1 h and cool down to room temperature at 20°C per min. A multimode atomic force microscopy (AFM) with Nanoscope V controller, (Veeco Ltd, USA) is used for all samples and magnetic force microscopy (MFM) in tapping mode is used to probe the magnetic domains and grain growth analysis of amorphous and polycrystalline CoFeB thin films. To perform four-probe electrical measurements, we deposit Ag/Cr contact pads on CoFeB thin films using the shadow mask technique. The Al wires bonded to the pads ensure ohmic contacts with equipotential surfaces.

3. Results and discussion

3.1. Magnetic force microscopy studies

The MFM micrographs of as-deposited CoFeB thin films of varying thicknesses (6, 9 and 36 nm) are presented in figure 1(a)–(c) and the corresponding AFM micrographs are shown in (d)–(f). We observe granular surface topography for all three films. Clearly, these morphological features dominate the magnetic signal measured by MFM. Therefore the MFM images look quite similar to surface topography. The MFM micrographs of annealed CoFeB thin films of varying thicknesses (6, 9 and 36 nm) are presented in figure 2(a)–(c) and the corresponding AFM micrographs are shown in (d)–(f). In contrast to as-deposited films, the annealed films are less granular. Therefore, the MFM images reveal the magnetic domain structures where the intensity of repulsive interaction (bright region) and the intensity of attractive interaction (dark region) are considered domains. The domain structures consist of irregular patches of varied shapes and sizes. The irregularly shaped domains may be due to grain growth formation in the amorphous matrix which was also confirmed by previously reported transmission electron microscope measurement results [20].

The magnetic domains found in annealed CoFeB thin films are greater than the grain size of 30-40 nm for 36 nm thin film. These large magnetic domains are formed due to strong exchange coupling interaction between the grains [22, 23]. The MFM images of the films show anisotropic magnetic domain contrasts for the smooth film, and the subsequent fragmentation of these domains as the roughness of the films increased. With increasing film thickness we observe larger magnetic domains.

3.2. Electrical transport

Figures 3(a) and (b) show the temperature-dependent four-probe sheet resistance, $R_\square(T)$ plots for both as-deposited and annealed CoFeB films. Clearly, all as-deposited films show non-metallic behavior, i. e. the resistance increases with decreasing temperature. On the other hand, we observe metallic behavior for annealed thin films. In addition, $R_\square(T)$ for the annealed thin film is smaller than that of the as-deposited film of the same

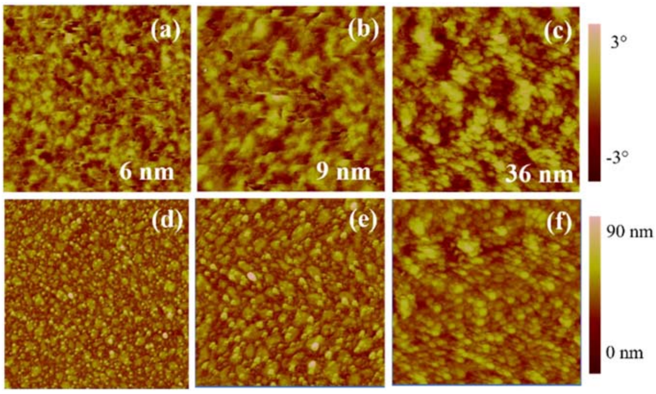

Figure 2. (a)–(c) The MFM images and the corresponding AFM images (d)—(f) with an area of 3 ×3 μm^2 for annealed CoFeB thin films of varying thicknesses 6, 9, and 36 nm respectively.

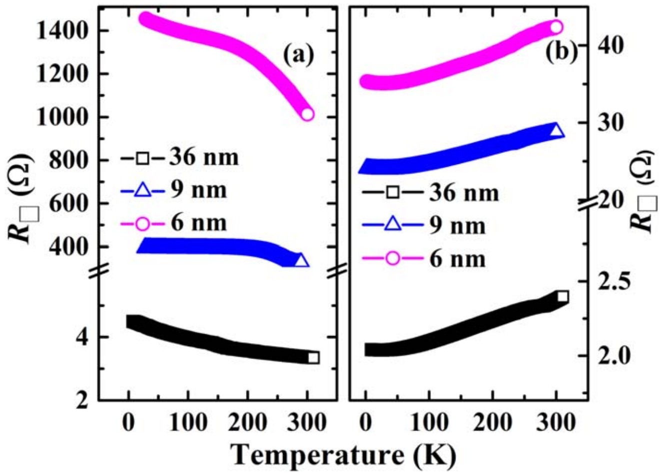

Figure 3. (a) The temperature-dependent sheet resistance, $R_{\square}$(T) plots for as-deposited and (b) annealed at 400°C CoFeB thin films of thicknesses 6 nm, 9 nm and 36 nm, respectively.

thickness revealing the non-metallic behavior for as-deposited and metallic behavior for annealed CoFeB thin films, respectively. These resistance values are comparable to the previously reported values in 23. The resistivity of annealed 36 nm film is found to be ≈ 8.6 $\mu\Omega$cm consistent with the resistivity of ≈8 $\mu\Omega$cm reported previously [20]. The larger $R_{\square}$(T) for amorphous films and observed non-metallic behavior are due to intra-grain tunneling and SiO_2 inclusions in the amorphous films which are confirmed by the previous reports on the effect of annealing on the electrical properties of polycrystalline CoFeB thin films [20, 23]. On the other hand, the metallic behavior of annealed thin films is due to the formation of nano-crystallites with electron scattering happening at grain boundaries. The post-growth annealing treatment of the as-deposited films improves the crystalline structure [20, 22–27]. This may reduce the grain boundaries and thus result in lower resistivity.

3.3. Magnetoresistance

Figure 4(a) and (b) show the magnetoresistance (MR) curves measured at 300 K and 10 K, respectively, for 36 nm annealed CoFeB thin film when the applied magnetic field is in longitudinal (parallel) and transverse (perpendicular) geometry to the sample plane. The negative MR values were observed in both parallel and perpendicular field geometry to the sample plane. A small hysteresis is found when the applied field is perpendicular to the film which is evident for the ferromagnetic behavior of annealed CoFeB thin film. The hysteresis is more prominent at low temperatures in the case of 50 K [see figure 5(a)] when the field is in perpendicular geometry to the sample plane. It is noted that the film has a slightly higher MR value at 10 K. The observed MR in the film through electronic transport is due to intragrain tunneling. Similar results on negative MR behavior were observed in the previous reports [16, 17]. In addition, we found that the thinner film has a larger MR value and the MR values remain almost temperature-independent as shown in figure 5(b).

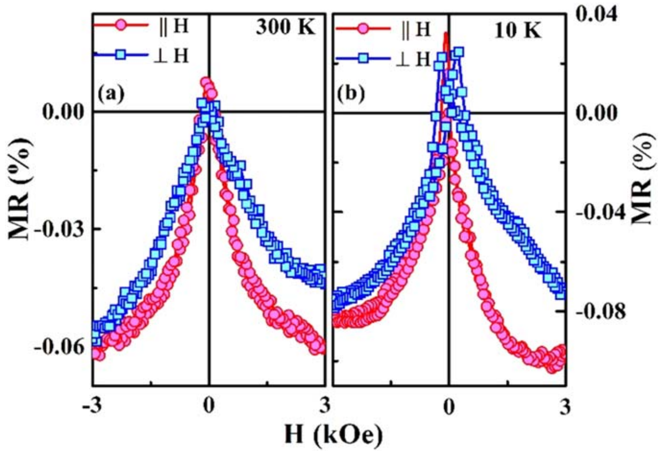

Figure 4. Magnetoresistance, $MR = (\rho(H) - \rho(0))$ x100/ $\rho(0)$ for 36 nm annealed CoFeB film at 300 K (a) and 10 K (b). $\rho(H)$ is the resistivity in the presence of a magnetic field, H applied parallel geometry to the film plane (red circles), and perpendicular geometry (blue squares).

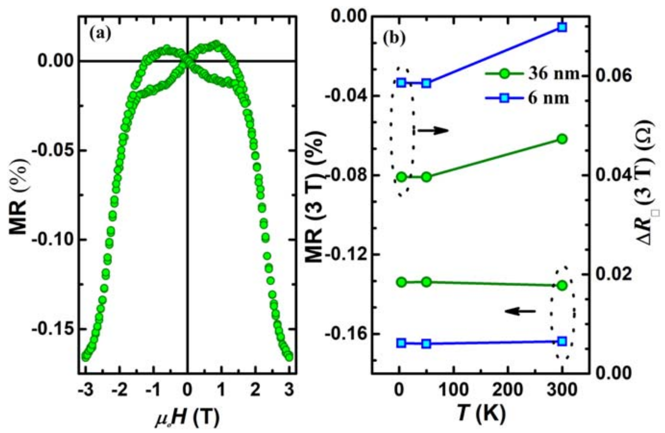

Figure 5. (a) Magnetoresistance, MR for 6 nm annealed CoFeB thin film measured at 50 K and (b) Temperature dependence of MR and $\Delta\rho = \rho(0) - \rho(H)$ at $\mu_o H = 3$T for 6 nm (blue squares) and 36 nm (green circles) annealed thin films.

In a granular system, the electronic transport at low temperatures depends significantly on the grain boundaries. As explained before, these boundaries act as a metallic barrier between ferromagnetic grains. With increasing magnetic fields, the grains gradually tend to align magnetically and, thus, the resistance reduces due to the conduction of spin-polarized charge carriers. The observed thickness dependence of MR can be explained in terms of the granularity of the film [16]. The MR measured at 50 K for a 6 nm thinner annealed CoFeB thin film is shown in figure 5(a). In the case of thinner films with smaller grains, the number of ferromagnetic grains within the mean free path is larger. Thus, the scattering events are higher and the MR is higher as compared to the case of thicker films with larger grains. Other granular alloys like Co-Cu and Co-Ag have displayed similar MR effects [14, 15, 28]. Figure 5(b) depicted the temperature-dependent MR for 6 nm and 36 nm thin films measured at 3T, which remain almost constant throughout the temperature range. The corresponding differences in the resistivity at 0 and 3T, $\Delta\rho$ are also shown in figure 5(b). With decreasing temperature, $\Delta\rho$ is reduced for both annealed films. At lower temperatures, the conduction electrons are more strongly spin-polarized due to larger magnetization and thus a larger decrease in resistance.

4. Conclusions

In summary, we have investigated PLD-grown CoFeB as-deposited and annealed thin films of varying thicknesses (6 to 36 nm) for magnetic domain structure, electrical conduction and magnetoresistance properties. The magnetic domain images probed using magnetic force microscopy revealed very large magnetic domains due to the interactions between the nanocrystalline grains in the annealed CoFeB thin films. The as-deposited thin films are non-metallic whereas the annealed thin films with growing granularity show metallic behavior. In comparison to thick films, higher MR values are observed in 6 nm annealed CoFeB thin film. We found an almost temperature-independent MR for both films. However, increasing magnetic fields reduces the resistivity due to the conduction of spin-polarized charge carriers. Our present study provides essential information on magneto-transport in crystalline CoFeB thin films in particular, which is eventually useful for the development of spintronic devices.

Acknowledgments

We thank Dr R K Rakshit for his guidance and Dr V Toutam for MFM measurements. We acknowledge the Council of Scientific and Industrial Research (CSIR) & Department of Science and Technology (DST), India for financial support.

Data availability statement

All data that support the findings of this study are included within the article (and any supplementary files).

ORCID iDs

G Venkat Swamy https://orcid.org/0000-0002-9911-0634
Himanshu Pandey https://orcid.org/0000-0002-7380-366X
G A Basheed https://orcid.org/0000-0003-4326-3356

References

[1] Ikeda S, Hayakawa J, Ashizawa Y, Lee Y M, Miura K, Hasegawa H, Tsunoda M, Matsukura F and Ohno H 2008 *Appl. Phys. Lett.* **93** 082508
[2] Ikeda S, Miura K, Yamamoto H, Mizunuma K, Gan H D, Endo M, Kanai S, Hayakawa J, Matsukura F and Ohno H 2010 *Nature Mater.* **9** 721
[3] Wang W G *et al* 2010 *Phys. Rev.* B **81** 144406
[4] Wang W G *et al* 2009 *Appl. Phy. Lett.* **95** 242501
[5] Lavrijsen R, Paluskar P V, Loermans C T J, van Kruisbergen P A, Kohlhepp J T, Swagten H J M, Koopmans B and Snoeck E 2011 *Journal of Appl. Phys.* **109** 093905
[6] Hayakawa J, Ikeda S, Lee Y M, Matsukura F and Ohno H 2006 *Appl. Phys. Lett.* **89** 232510
[7] Djayaprawira D D, Tsunekawa K, Nagai M, Maehara H, Yamagata S, Watanabe N, Yuasa S, Suzuki Y and Ando K 2005 *Appl. Phys. Lett.* **86** 092502
[8] Yang Y, Wang W X, Yao Y, Liu H F, Naganuma H, Sakul T S, Han X F and Yu R C 2012 *Appl. Phys. Lett.* **101** 012406
[9] Zhang Y, Mi W B and Zhang X X 2016 *EPL* **114** 67003
[10] Su J, Li G, Bai H, Zhu Z Z, Zhang Y, Kang S S, Zhu T and Cai J W 2020 *J. Phys. D: Appl. Phys.* **53** 125003
[11] Bivas R, Katsuya M, Hiromasa T and YoshiChika O 2020 *J. Phys. Condens. Matter* **32** 414002
[12] Yamamoto T *et al* 2022 *J. Phys. D: Appl. Phys.* **55** 275003
[13] Gao L, Jiang X, Yang S-H, Rice P M, Topuria T and Parkin S S P 2009 *Phys. Rev. Lett.* **102** 247205
[14] Gerber A, Milner A, Groisman B, Karpovsky M and Gladkikh A 1997 *Phys. Rev.* B **55** 6446–52
[15] Xiao John Q, Samuel Jiang J and Chien C L 1992 *Phys. Rev.* B **46** 9266 (R)
[16] Johnsson P, Aoqui S-I and Grishin A M 2003 *J. Appl. Phys.* **93** 8101
[17] Kalinin Y E, Sitnikov A V, Stognei O V, Zolotukhin I V and Neretin P V 2001 *Materials Science and Engineering* A **304–306** 941
[18] Bhutta K M and Reiss G 2010 *Journal of Appl. Phys.* **107** 113718
[19] Rüffer D *et al* 2014 *APL Mater.* **2** 076112
[20] Swamy G *et al* 2013 *AIP Adv.* **3** 072129
[21] Geet A, Chris C, Laura S, Guru V, Kelly M, Zhaoxia Z and Dirk B 2020 *Mater. Res. Express* **7** 106406
[22] Deo N, Bain M F, Montgomery J H and Gamble H S 2005 *J. Mater. Sci, Mater. Electron.* **16** 387392
[23] Venkat Swamy G, Rout P K, Singh Manju and Rakshit R K 2015 *J. Phys. D: Appl. Phys.* **48** 475002
[24] Gupta N K *et al* 2022 *J. Magn. Magn. Mater.* **562** 169799
[25] Jhajhria D, Pandya D K and Chaudhary S 2018 *J. Alloys Compd.* **763** 728–35
[26] Minghua L, Hui S, Yuegang D, Lei D, Gang H, Yao Z, Ye L and Guanghua Y 2017 *J. Magn. Magn. Mater.* **439** 17
[27] Anupam J P C, Rout P K, Hossain Z and Budhani R C 2010 *J. Phys. D: Appl. Phys.* **43** 255002
[28] Kalita V M, Timopheev A A, Lozenko A F, Ryabchenko S M, Los A V, Stognei O V and Sitnikov A V 2011 *Journal of Appl. Phys.* **110** 113918